Available online at www.sciencedirect.com
SCIENCE DIRECT®
International Journal of Plasticity 22 (2006) 257–278
INTERNATIONAL JOURNAL OF Plasticity
www.elsevier.com/locate/ijplas

A molecular dynamics study of void growth and coalescence in single crystal nickel

G.P. Potirniche [a], M.F. Horstemeyer [a,b,*], G.J. Wagner [c], P.M. Gullett [d]

[a] *Center for Advanced Vehicular Systems, Mississippi State University, 206 Carpenter Bldg., P.O. Box ME, Mississippi State, MS 39762, USA*
[b] *Department of Mechanical Engineering, Mississippi State University, 206 Carpenter Bldg., P.O. Box ME, Mississippi State, MS 39762, USA*
[c] *Sandia National Laboratories, Livermore, CA, USA*
[d] *Civil Engineering Department, Mississippi State University*

Received 5 June 2004
Available online 17 May 2005

Abstract

Molecular dynamics simulations using Modified Embedded Atom Method (MEAM) potentials were performed to analyze material length scale influences on damage progression of single crystal nickel. Damage evolution by void growth and coalescence was simulated at very high strain rates (10^8–10^{10}/s) involving four specimen sizes ranging from ≈5000 to 170,000 atoms with the same initial void volume fraction. 3D rectangular specimens with uniform thickness were provided with one and two embedded cylindrical voids and were subjected to remote uniaxial tension at a constant strain rate. Void volume fraction evolution and the corresponding stress–strain responses were monitored as the voids grew under the increasing applied tractions.

The results showed that the specimen length scale changes the dislocation pattern, the evolving void aspect ratio, and the stress–strain response. At small strain levels (0–20%), a damage evolution size scale effect can be observed from the damage-strain and stress–strain curves, which is consistent with dislocation nucleation argument of Horstemeyer et al. [Horstemeyer, M.F., Baskes, M.I., Plimpton, S.J., 2001a. Length scale and time scale effects on the

* Corresponding author. Tel.: +1 662 325 7308; fax: +1 662 325 7223.
E-mail address: mfhorst@me.msstate.edu (M.F. Horstemeyer).

0749-6419/$ - see front matter
doi:10.1016/j.ijplas.2005.02.001

plastic flow of FCC metals. Acta Mater. 49, pp. 4363–4374] playing a dominant role. However, when the void volume fraction evolution is plotted versus the applied true strain at large plastic strains (>20%), minimal size scale differences were observed, even with very different dislocation patterns occurring in the specimen. At this larger strain level, the size scale differences cease to be relevant, because the effects of dislocation nucleation were overcome by dislocation interaction.

This study provides fodder for bridging material length scales from the nanoscale to the larger scales by examining plasticity and damage quantities from a continuum perspective that were generated from atomistic results.

Keywords: Molecular dynamics; Embedded atom method; Void growth; Void coalescence; Nickel single crystal

1. Introduction

Metal components commonly fail by nucleation, growth and coalescence of voids. This type of mechanical failure, intrinsically a multiscale process, occurs by damage progression and involves mechanisms that have been extensively studied at the micro- and macroscales. However, at small material length scales (nanometers) the mechanisms of void growth and void coalescence have not been satisfactorily studied and understood, mainly because of the lack of materials characterization methods at that scale.

At the macroscale ductile failures of engineering alloys have been studied extensively (Lemaitre, 1992; Tvergaard, 1990), and they can be characterized by a progressive accumulation of cavities, voids, or cracks inside the material, designated as *damage*, or sometimes called porosity or void volume fraction. Due to the damage induced in the material, the load carrying capacity is significantly diminished. Damage was first introduced as a scalar parameter, ϕ (Kachanov, 1958; Rabotnov, 1969). The damage ϕ was algebraically defined as $\phi = V_v/V$, where V_v is the volume of voids, and V is the volume of the aggregate material. Due to the increased effective stress, new voids are nucleated inside the material. When the void volume fraction is increased a typical stress–strain curve will experience softening due to specimen necking, thus, reducing the ability to carry load under the same applied strain. The increase in void volume fraction during plastic deformation is basically due to three mechanisms: nucleation, growth and coalescence of voids. This particular study is focused on the mechanisms of void growth and void coalescence.

As voids initiate in the material under applied loads, the deterioration process continues with the void growth, and later, with the void coalescence. From a macroscopic perspective, the most studied mechanism has been void growth with a focus on different parameters such as strain rate effects (Cocks and Ashby, 1980, 1982; Budianski et al., 1982; McClintock, 1968), work hardening effects (Rice and Tracey, 1969) and plastic flow localization in single crystals (Shu, 1998). Recent micromechanical studies performed on planar models examined the influence of different

initial void volume fractions and different stress triaxialities (Faleskog and Shih, 1997; Cuitino and Ortiz, 1996; Moran et al., 1990).

Void coalescence is also an important damage mechanism and can be defined in different ways. Finite element analyses of the coupled effect of void growth and coalescence were performed by Horstemeyer et al. (2000a) and indicated that a parameter named critical intervoid ligament distance (ILD) determines the point of coalescence. Tvergaard and Niordson (2004) considered the interaction between the large and small voids and found that, at size lengths comparable with material length scale, the small void growth is drastically limited by the stress concentration effect of large voids. Tvergaard and Needleman (1995, 1997) and Ramaswamy and Aravas (1998) have discussed void coalescence from a macroscale continuum perspective using an intrinsic special size scale parameter. Pardoen et al. (1998) used four different coalescence criteria in finite element simulations and by comparing these results to experimental data for copper they concluded that a critical void growth rate is inversely related to the triaxiality. Nagaki et al. (1993) examined void growth by coalescence from using different neighbor distances in a numerical setting. Benson (1993, 1995) has numerically analyzed different void configurations (coalescence) for high strain rate shock environments finding that void coalescence and configuration of the fracture surface are function of the tension wave. Recent physical experiments from the studies in the materials science literature reveal a strong influence of coalescence on final fracture of materials (Worswick and Pick, 1995; Geltmacher et al., 1996, 1998; Zurek et al., 1997; Tonks et al., 1997; Bandstra et al., 1998; Lu et al., 1998) mainly by void impingement. During void impingement, the material ligament between two voids necks to a point as two neighbors grow together (Cottrell, 1959). The void sheet mechanism occurs by another mechanism. Primary voids usually nucleate from second phase particles, and these particles grow when the material is plastically deformed. At a higher strain/stress level, neighboring particles will nucleate secondary particles. These particles tend to be smaller and tend to have stronger bonds with the matrix. Then, voids from the larger particle distributions will link under localized shearing to a smaller void distribution through the ligament over a small interval of strain. The material path between void distributions looks sheet-like. Recently, Chien et al. (2004) used a combination of a plane stress description of necking and plane strain formulation of shear localization, and correlated forming diagram limits for two aluminum alloys under biaxial stretching conditions. Void size effect on the evolution of the void volume fraction during void growth was examined at macroscale by Wen et al. (2005), and they concluded that under uniaxial tension, the stress–strain curve is significantly influenced at larger void volume fractions. Void nucleation and growth in polycrystalline materials was investigated by Bonfoh et al. (2004) by using a two-level homogenization approach, considering that nucleation occurs at inclusion particles by storage of elastic strain energy in the inclusion particle and deriving the equivalent behavior of single crystals with voids.

In this study, we focus on single voids growing and multiple voids coalescing at the nanoscale by MEAM potentials in molecular dynamics simulations. Molecular dynamics has become a very useful computational method for simulating elasto-plastic deformation and failure processes at the nanoscale. The dimensions for the

specimens tested with this method are situated in the range of nanometers, while the number of atoms can vary from a few hundred to a few hundred thousand. The main shortcoming of molecular dynamics is that the method is computationally intensive, requiring long solution time and parallel processing. However, with the development of computational tools, molecular dynamics methods have become an integral part of a multiscale engineering approach of failure in materials.

Previous research (Horstemeyer et al., 2001b; Gall et al., 2000) indicated that molecular dynamics can be used to study plastic deformation mechanisms and the phenomenon of ductile failure at the atomistic scale. Horstemeyer et al. (2001a) integrated molecular dynamics in a multiscale modeling approach and analyzed the intrinsic mechanical response of single crystals at three relevant material scales. The results indicated that the material length scale greatly influenced the stress–strain response. As the specimen size increased the yield stress decreased as a function of volume per surface area. By analyzing void growth mechanisms in copper single crystals using both molecular dynamics and crystal plasticity theory Farrissey et al. (2000) found that while a qualitative similitude between void developments at atomic and crystallographic length scales exists, the atomistic simulations indicated that the stress levels predicted with molecular dynamics are larger than those predicted with crystal plasticity, consistent with the dislocation nucleation arguments of Horstemeyer et al. (2001a); Horstemeyer (2001); Horstemeyer et al. (2001b). Makino et al. (2000) simulated void formation in nickel single crystals using molecular dynamics by subjecting infinitely long cylinders to a multiaxial tensile strain field. Their work was chiefly concerned with void nucleation and stable void growth, and they found that above a critical value of the applied load, a void nucleated from vacancies in the crystalline lattice. However, they did not study size scale effects in their molecular dynamics simulations.

The contribution of this work was to perform a systematic investigation of the void growth and void coalescence mechanisms in single crystals nickel under uniaxial strain field and at increasing material length scales with the purpose to understand continuum quantities that arose from molecular dynamics simulations. The stress–strain responses of specimens with one or two voids were simulated for specimens with an increasing number of atoms. The void volume fraction evolution was determined as a function of the applied strain for single and multiple void specimens.

2. Modified embedded atom method background

The MEAM potential employed in a computational framework can be used to determine the relationships between microstructure and mechanical properties at material scales ranging from atomic to continuum (Baskes and Johnson, 1994; Baskes, 1994, 1997). Recent studies (Horstemeyer and Baskes, 1999; Horstemeyer et al., 2002, 2003; Horstemeyer, 2001) have investigated size scale effects with the yield strength and the kinematics of deformation. Atomistic simulations were shown to give results that agree well with the phenomenological attributes of plasticity observed in macroscale experiments (Horstemeyer, 2001). Some of the main findings

include strain rate dependence of the flow stress into a rate independent regime, approximate Schmid type behavior, size scale dependence on the flow stress, and kinematic behavior of large deformation plasticity.

The MEAM potential is based on molecular dynamics principles developed initially by Daw and Baskes (1984). MEAM allows the calculation of the thermodynamic forces and stress tensors for the atoms in the lattice based on the notion of embedded energy. The total energy of an atomic system, E, is calculated by summing the individual embedding energy F^i of each atom i in the atomic aggregate, as follows:

$$E = \sum_i F^i \left(\sum_{j \neq i} \rho^i(r^{ij}) \right) + \frac{1}{2} \sum_{ij} \phi^{ij}(r^{ij}), \tag{1}$$

where, j is any neighboring atom, r^{ij} and ϕ^{ij} are the distance and the pair potential, respectively, between the atoms i and j.

Next, the force between any pair of two atoms i and j is derived from the embedding energy as

$$f_\alpha^{ij} = \frac{\partial E}{\partial r^{ij}} \frac{r_\alpha^{ij}}{r^{ij}}, \tag{2}$$

where the subscript α is the directional component. The dipole force tensor at each atom i is given by

$$\beta_{km}^i = \frac{1}{\Omega^i} \sum_{j \neq i}^{N} f_k^{ij} r_{km}^{ij}, \tag{3}$$

where N is the number of nearest neighbor atoms and Ω^i is the atomic volume. The stress for the system of atoms is defined as a volume average of the dipole force tensor

$$\sigma_{mk} = \frac{1}{N^*} \sum_{i}^{N^*} \beta_{mk}^i, \tag{4}$$

where N^* is the number of active atoms that participate in creating the stress in the lattice.

For a more detailed explanation of the MEAM potentials constitutive equations, the reader is referred to Baskes (1994, 1997).

3. Specimen setup for void growth and void coalescence studies

Void growth and coalescence were studied using four specimens of increasing size in FCC single crystal nickel using MEAM potentials. For void growth study purposes, we used specimens representing a plate with a central hole subjected to uniaxial strain rate as shown in Fig. 1. The four specimen sizes were obtained by increasing the length and the width of the specimen. Consequently, the resulting specimens

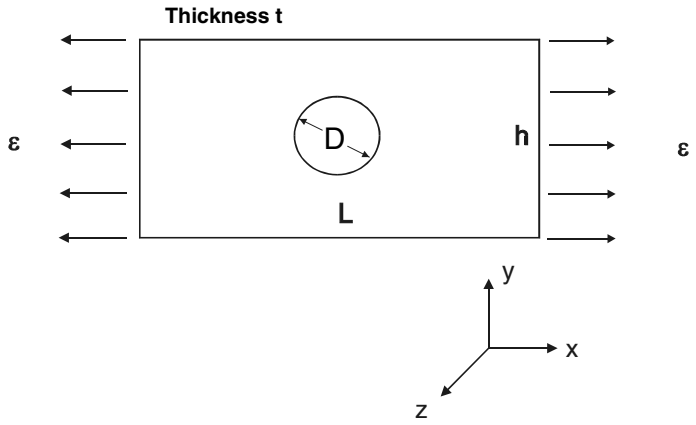

Fig. 1. Geometry of void growth specimen subjected to uniaxial tension under constant strain rate.

contained a number of atoms that varied from $N = 4408$ atoms (smallest length scale) to $N = 171{,}376$ atoms (largest length scale). Geometrical dimensions corresponding to these four length scales are indicated in Table 1. All the specimens were assigned the same thickness of 0.992 nm. For all the one-void specimens, the ratios of geometrical dimensions were constant $h/L = 0.76$ and $D/L = 0.17$. For the two-void specimens the ratio were $h/L = 0.76$ and $D/L = 0.125$. Each specimen was provided with a thickness of four atomic distances.

To analyze the mechanism of void coalescence, two-void specimens at four increasing length scales similar to the one-void specimens were analyzed. These two-void specimens are presented in Fig. 2. The geometrical dimensions associated with the two-void specimens are indicated in Table 2. The two-void specimens were built considering the same amount of initial void volume fraction as the one-void specimens, for the same length scale. Each of the two voids has a diameter D, with an intervoid distance also equal also to D. The four specimens sizes resulted with a number of atoms ranging from $N = 5052$ atoms to $N = 175{,}172$ atoms.

The models were chosen so that the geometrical dimensions for both one-void and two-void specimens ranged from a few nanometers to tens of nanometers. Thus, the mesh sizes represent a variety of length scales in which damage processes occur. The specimen edges were aligned with the global system of coordinates (xyz). The FCC

Table 1
Geometrical dimensions of void growth specimen subjected to uniaxial tension under constant strain rate

Specimen	L (nm)	h (nm)	t (nm)	D (nm)	Number of atoms
1	8.448	6.4963	0.992	1.493	4408
2	16.896	12.992	0.992	2.986	18,448
3	33.792	25.985	0.992	5.973	75,648
4	50.688	38.977	0.992	8.960	171,376

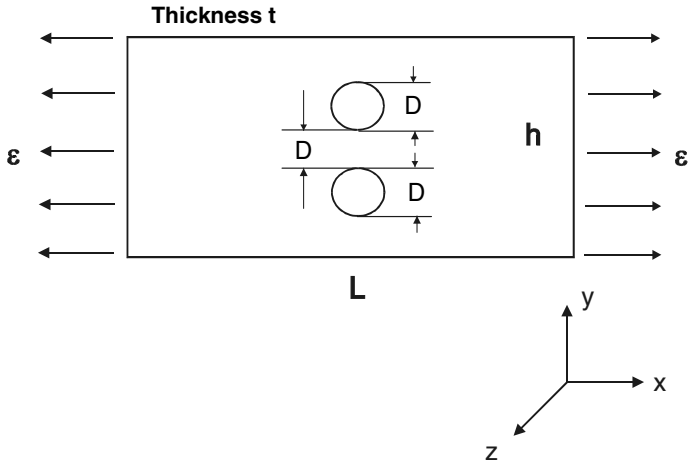

Fig. 2. Geometry of void coalescence specimen subjected to uniaxial tension under constant strain rate.

Table 2
Geometrical dimensions of void coalescence specimen subjected to uniaxial tension under constant strain rate

Specimen	L (nm)	h (nm)	t (nm)	D (nm)	Number of atoms
5	8.448	6.4963	0.992	1.056	5052
6	16.896	12.992	0.992	2.112	19,748
7	33.792	25.985	0.992	4.224	78,140
8	50.688	38.977	0.992	6.336	175,172

crystalline lattice was aligned for all one-void and two-void specimens similarly, that is, the x-axis corresponded to (1 0 0) direction, the y-axis corresponded to (0 1 1) direction and the z-axis corresponded to (0 −1 1) direction. The applied boundary conditions are indicated in Figs. 1 and 2. The applied tractions were exerted in the x-direction as a strain rate, up to a total true strain of $\varepsilon = 41\%$. The upper and the lower edges of the specimen were free to move. Most of the results presented here were obtained by simulating a strain rate of 10^{10}/s. We also analyzed the influence of strain rate on the stress–strain diagram for one-void and two-void specimens by simulating two additional strain rates of 10^8 and 10^9/s. All the simulations were run at a constant temperature of 300 K.

4. Results and discussion

This section presents results regarding the stress–strain and void volume fraction response of nanomechanical specimens with one- and two-voids and void volume fraction evolution with respect to the applied strain. The influence of strain rate on the stress–strain response is also analyzed in the latter part of this section.

4.1. Void growth

Due to the nature of the MEAM using molecular dynamics principles, very high strain rates were considered for the analyses; otherwise, extremely large computational times were required to achieve solution. As stated by Horstemeyer et al. (2001a), the computational platform determines the upper atomic length scale; consequently, there is a trade-off between the atomistic specimen size and the strain rate. For the purpose of studying void growth mechanisms, we first considered a strain rate of 10^{10}/s. The specimens were subjected to uniaxial tension until the total remote applied strain reached 41% true strain. Failure by void growth has been noticed for both one- and two-void specimens. The uniaxial stress–strain behavior was quantified, and the results are presented in Figs. 3–6.

The stress–strain curve of the one-void specimens for the first two increasing length scales are presented in Fig. 3 (for $N = 4408$ atoms) and Fig. 4 (for $N = 18{,}448$ atoms) indicating the stages of the specimens' internal evolution of damage. In these plots, we use the centrosymmetry parameter defined by Kelchner et al. (1998) to highlight the dislocations in the specimen. This parameter for each atom is given by:

$$P = \sum_i |\mathbf{R}_i + \mathbf{R}_{i+6}|^2, \tag{5}$$

where $\mathbf{R}_i$ and $\mathbf{R}_{i+6}$ are the vectors corresponding to the six pairs of opposite nearest neighbors in the fcc lattice; thus, $P = 0$ in an undisturbed portion of the lattice, and P becomes large near dislocations or free surfaces. In these figures, only those atoms with $P \geqslant 2.0$ are plotted, giving a rough picture of the dislocation pattern in the specimen.

From Fig. 3 can be observed that the uniaxial stress–strain response for the one-void specimen at the lowest material length comprises an elastic portion up to a true strain of 14.5% and a value of the yield strength of about 20.5 GPa. As the yield strength is reached first, dislocations nucleate near the void due to the stress concentration effect. By increasing the applied strain more dislocations are initiated from the hole and propagate toward the edges of the specimen. At the same time, the void increases in volume, leading to an increase in the void volume fraction. The aspect ratio of the hole also changes noticeably due to dislocations being nucleated from the void and from the plastic spin occurring at larger strains. Also, the stress resistance of the specimen decreases significantly to about 5 GPa at the final true strain of 41%. Severe necking of the specimen occurs starting at about 25% strain level. Fig. 4 presents the stress–strain response for the one-void specimen and the next largest specimen size ($N = 18{,}448$ atoms). Fig. 4 also indicates that the dislocation pattern for the larger specimen is different than the dislocation pattern observed in the case of the smallest material length scale. As the length scale increases, by comparing Figs. 3 and 4, the yield strength decreases from about 20.5 GPa to about 16.7 GPa. As in the case of first material length scale, dislocations nucleate from the void toward the edges of the specimen. The location of the severe necking is slightly repositioned compared with the specimen of the first length scale. Also,

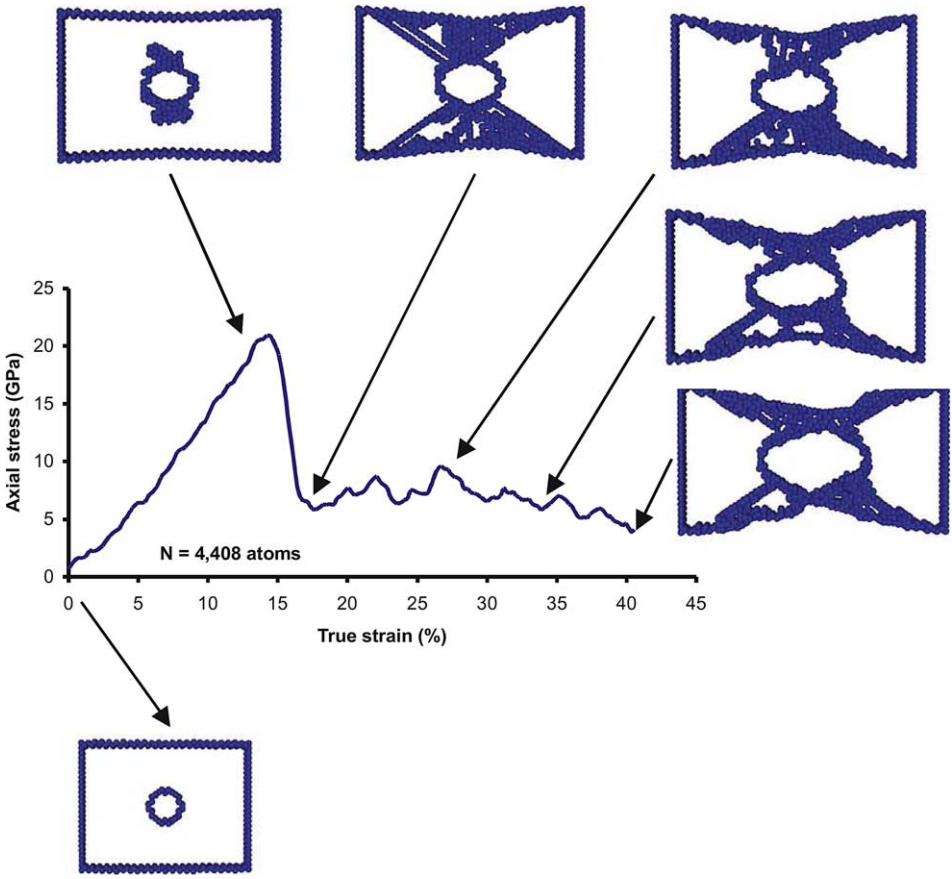

Fig. 3. Average stress versus true strain curve at 10^{10}/s strain rate for the one-void nickel specimen with N = 4,408 atoms.

another interesting feature is that the aspect ratio of the void is highly influenced by the dislocation pattern emanating from the hole and significantly different than in the previous smaller material length scale specimen. The increase in void volume fraction and dislocations nucleation induces an abrupt decrease in the capacity of the specimen to respond to stress due to uniaxial straining. In the case of 18,448 atoms, the stress–strain curve is smoother compared with the previous length scale of 4408 atoms. This effect is due to the atomic vibrations that have a greater influence at the smaller length scales and tend to influence the averaged values of stress.

4.2. Void coalescence

To study the coalescence effects at atomistic length scales and under very high rate of straining, similar uniaxial tension experiments were performed for the two-void specimens shown in Fig. 2. Similar to the case of the one-void specimen, four increasing

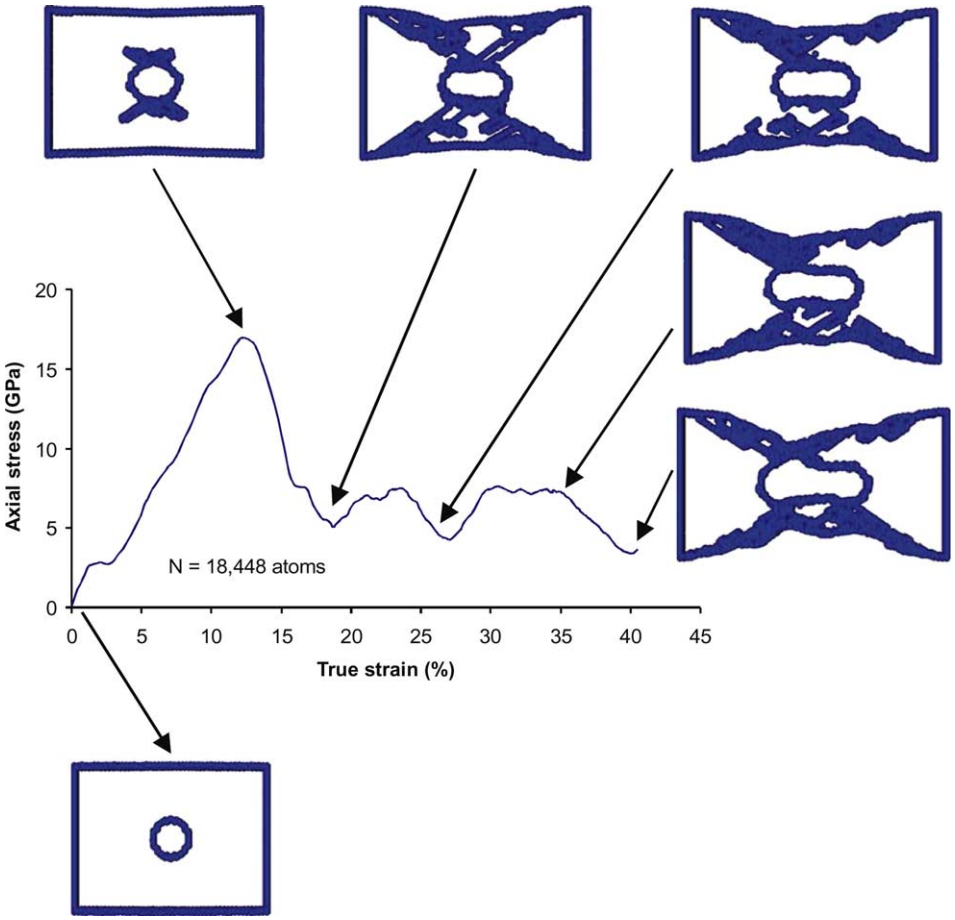

Fig. 4. Average stress versus true strain curve at 10^{10}/s strain rate for the one-void nickel specimen with N = 18,448 atoms.

length scales were simulated, in an effort to understand the length scale effect on void coalescence mechanism. As indicated in Table 2, the length scales considered ranged from 5052 to 175,172 atoms, or from a few tens of nanometers to about half a micron.

Fig. 5 shows the dislocation motion as a function of the stress–strain response indicating a yield stress of 18.92 GPa (at 14.9% strain) for the lowest material length scale (N = 5052 atoms). As the uniaxial stress reaches the yield stress value, dislocations are noticed to nucleate in the ligament region between the two voids. As the applied strain increased, the region between the two voids shrank, and the two voids collapsed to form one larger void. Concomitantly, dislocations nucleated toward the edges of the specimen, causing the initial necking of the tensile specimen. The stress–strain diagram also indicated that the largest drop in the stress–strain curve occurred

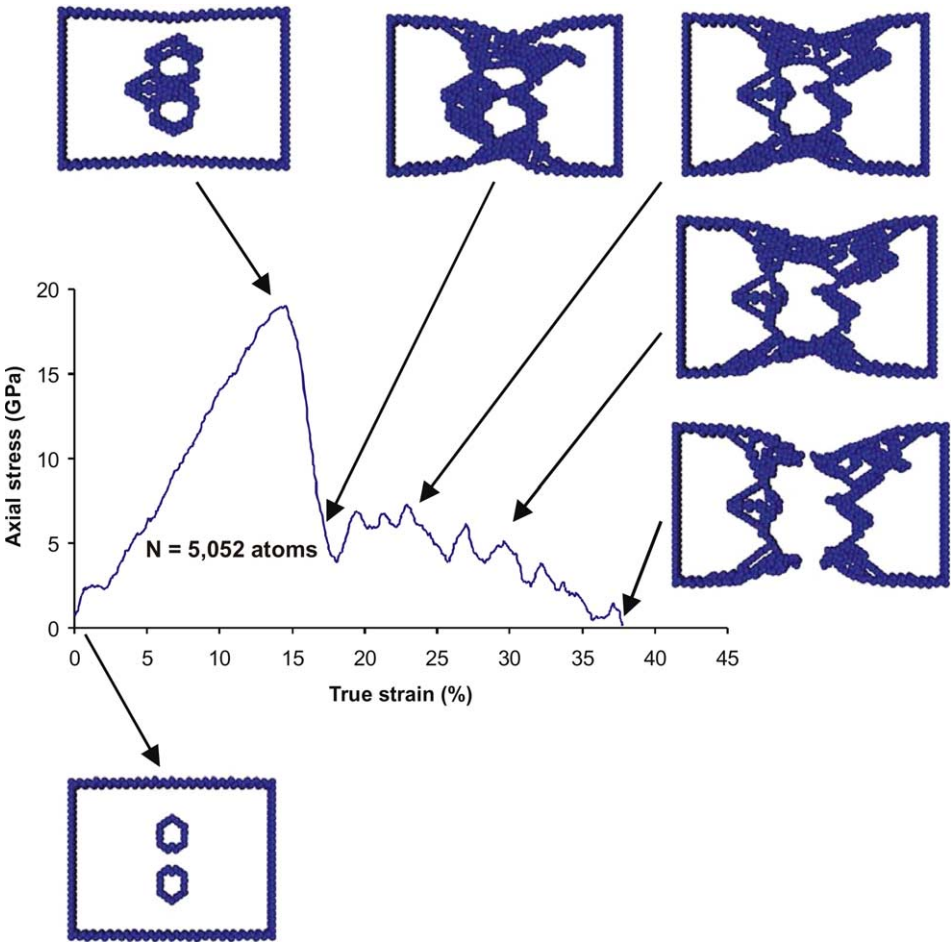

Fig. 5. Average stress versus true strain curve at 10^{10}/s strain rate for the two-void nickel specimen with N = 5,052 atoms.

as the voids coalesced to form one larger void. Furthermore, as the applied strain increased, the coalesced voids increased their volume. At the same time, nucleated slip patterns further decreased the stress resistance of the uniaxial specimen.

For the next increasing length scale, the uniaxial stress–strain curve from Fig. 6 indicated that the initial yield strength decreased to 15.37 GPa with a corresponding total true strain of 12.11%. As in the case of the previous material length scale, dislocations nucleated in the ligament region between the two voids, which resulted in their coalescence and a very sudden drop in the stress–strain curve. Also, dislocations emanated toward the outer edges of the specimen. Void coalescence caused an increase in the dislocation nucleation process and necking as the specimen is strained up to 41% true strain.

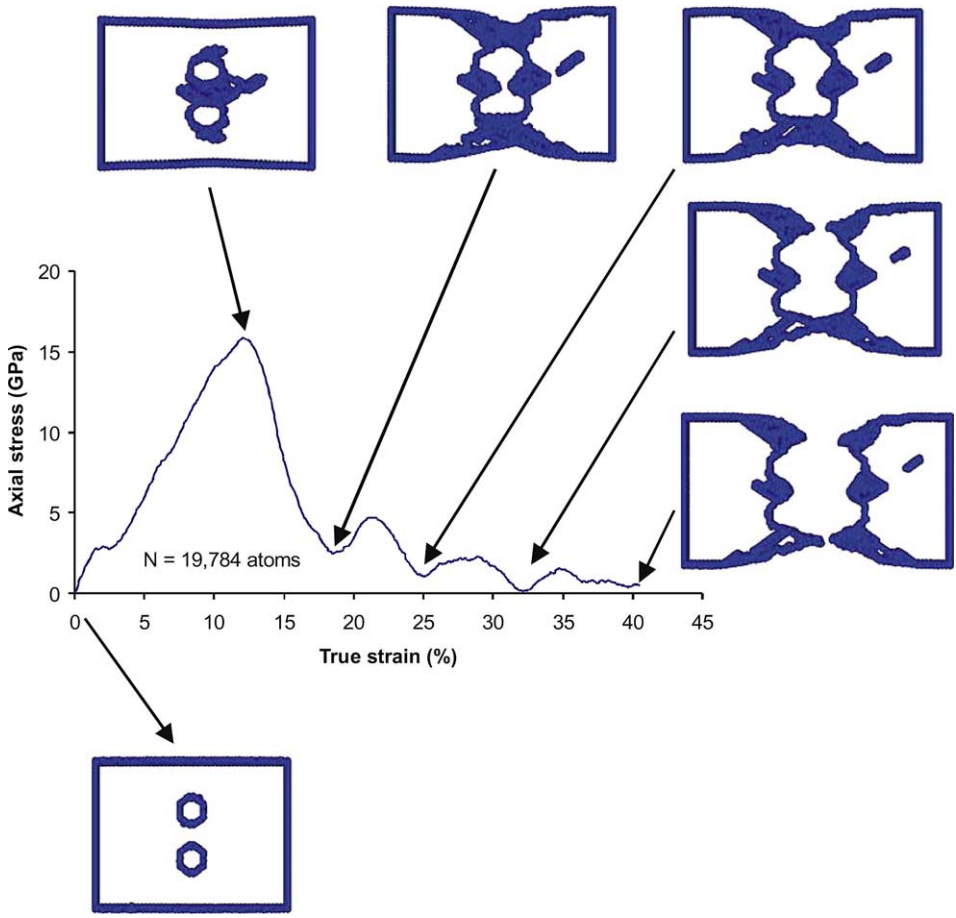

Fig. 6. Average stress versus true strain curve at 10^{10}/s strain rate for the two-void nickel specimen with N = 19,784 atoms.

4.3. Void volume fraction evolution

Void volume fraction has been computed during uniaxial straining for all one-void and two-void nickel specimens. The simulation results, shown in Fig. 7(a) and (b) indicate that, for both the one-void specimens and two-void specimens, under increasing uniaxial strain, the void volume fraction (f) for the one-void specimens increases from 0.03 to a maximum value of about 0.3 for all four material length scales analyzed. However, the void volume fraction varied for the early straining up to about 20% true strain. In general, the smaller length scale specimen experienced an increased void-volume fraction resulting from larger elastic stresses. This void volume size scale effect could also be influenced by the differences in the dislocation nucleation pattern. As the strain is increased and large plastic deformation occurs, the length scale effect diminished to the point where the four increasing

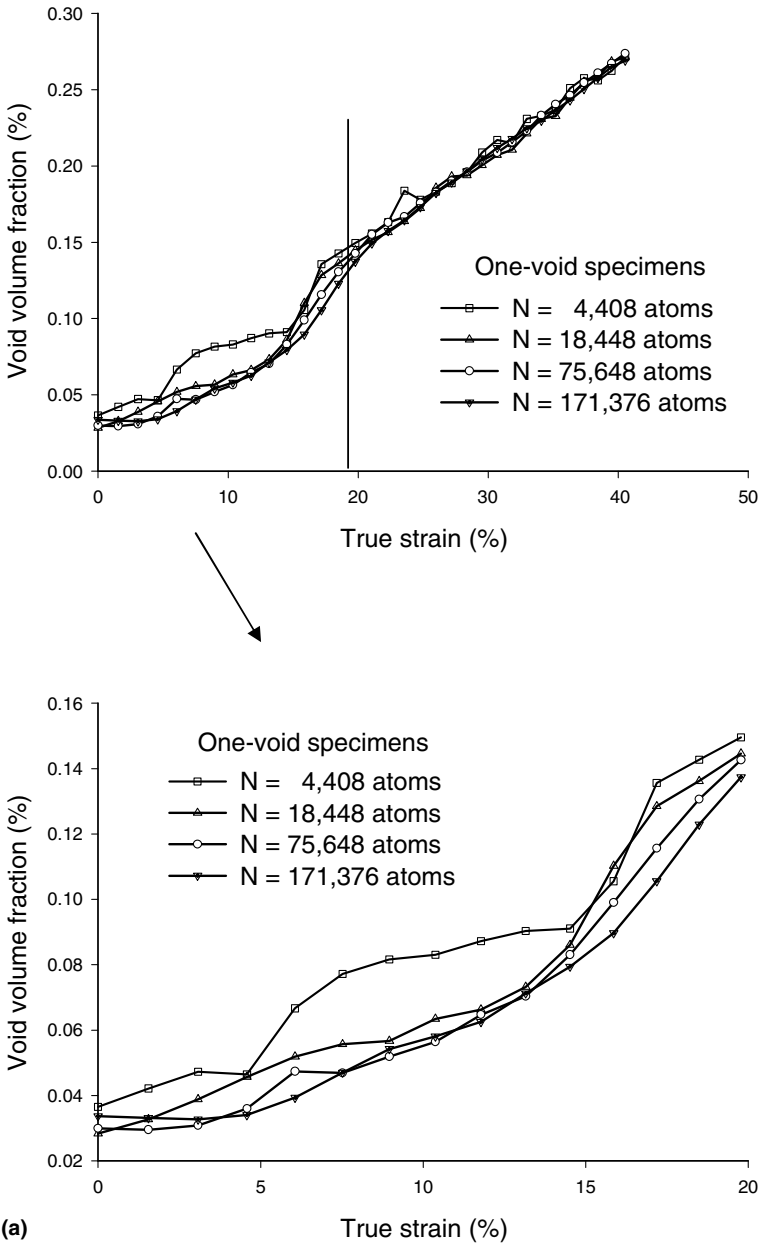

Fig. 7. Evolution of void volume fraction during uniaxial straining (10^{10}/s strain rate) for: (a) one-void specimens; (b) two-void specimens.

length scale specimens present almost the same void volume fraction with respect to the applied uniaxial strain up to the final applied strain. Early on, dislocations nucleating give a size scale trend but when dislocations are moving and interacting, no size

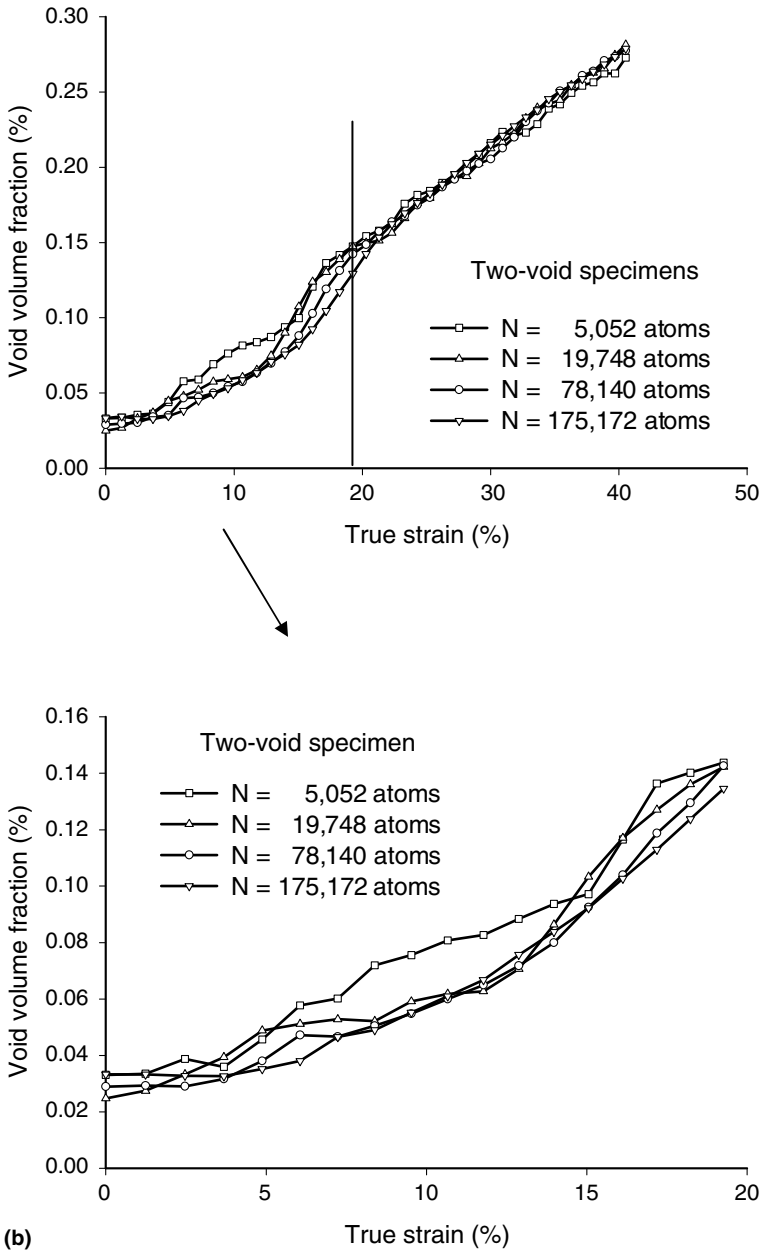

Fig. 7 (*continued*)

scale trend is observed. Another way of stating this is that when the ratio of elastic to plastic strains is high, a length scale effect is observed, but when the elastic to plastic ratio is low, no length scale effect is observed.

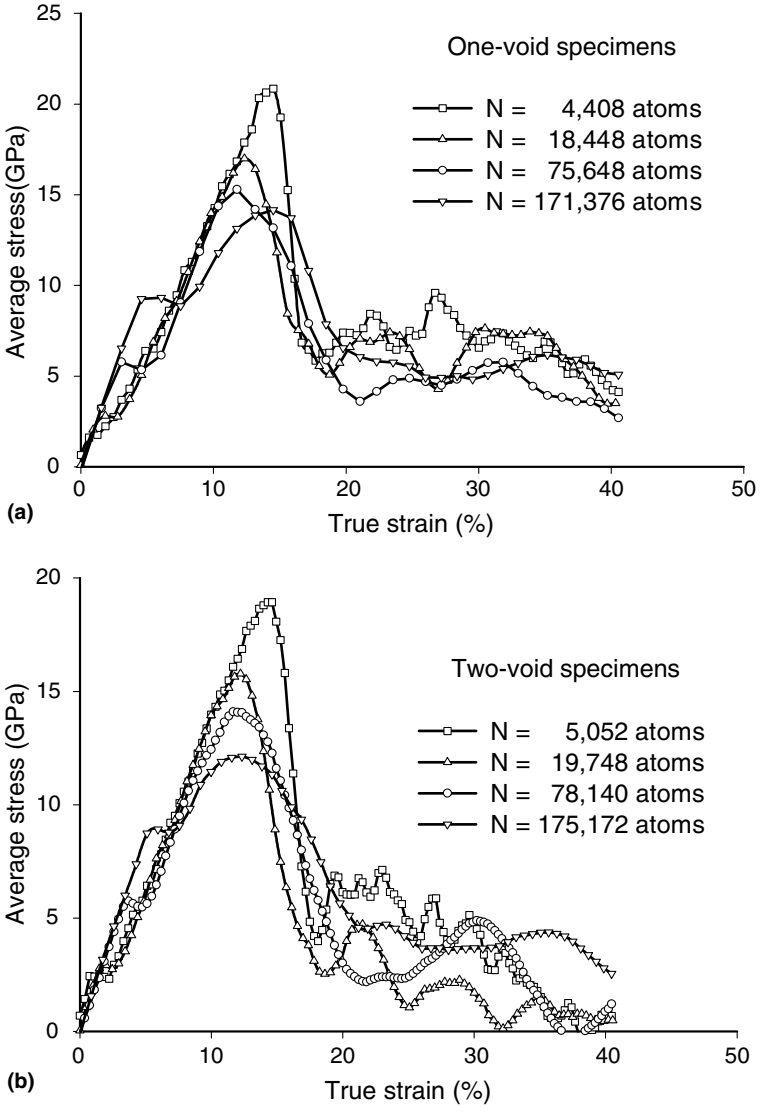

Fig. 8. Comparison of average stress versus true strain response (10^{10}/s strain rate) at increasing material length scale: (a) one-void specimen; (b) two-void specimens.

The same conclusions can be drawn from observing Fig. 7(b), where the void volume fraction (f) evolution with respect to the applied uniaxial strain is presented for the two-void specimens. For these specimens, void-volume fraction varies from about 0.03 to about 0.3. As in the case of one-void specimens, the main difference in void volume fraction with respect to the applied strain between increasing length scale for the two-void specimens is also obtained during the loading at moderate

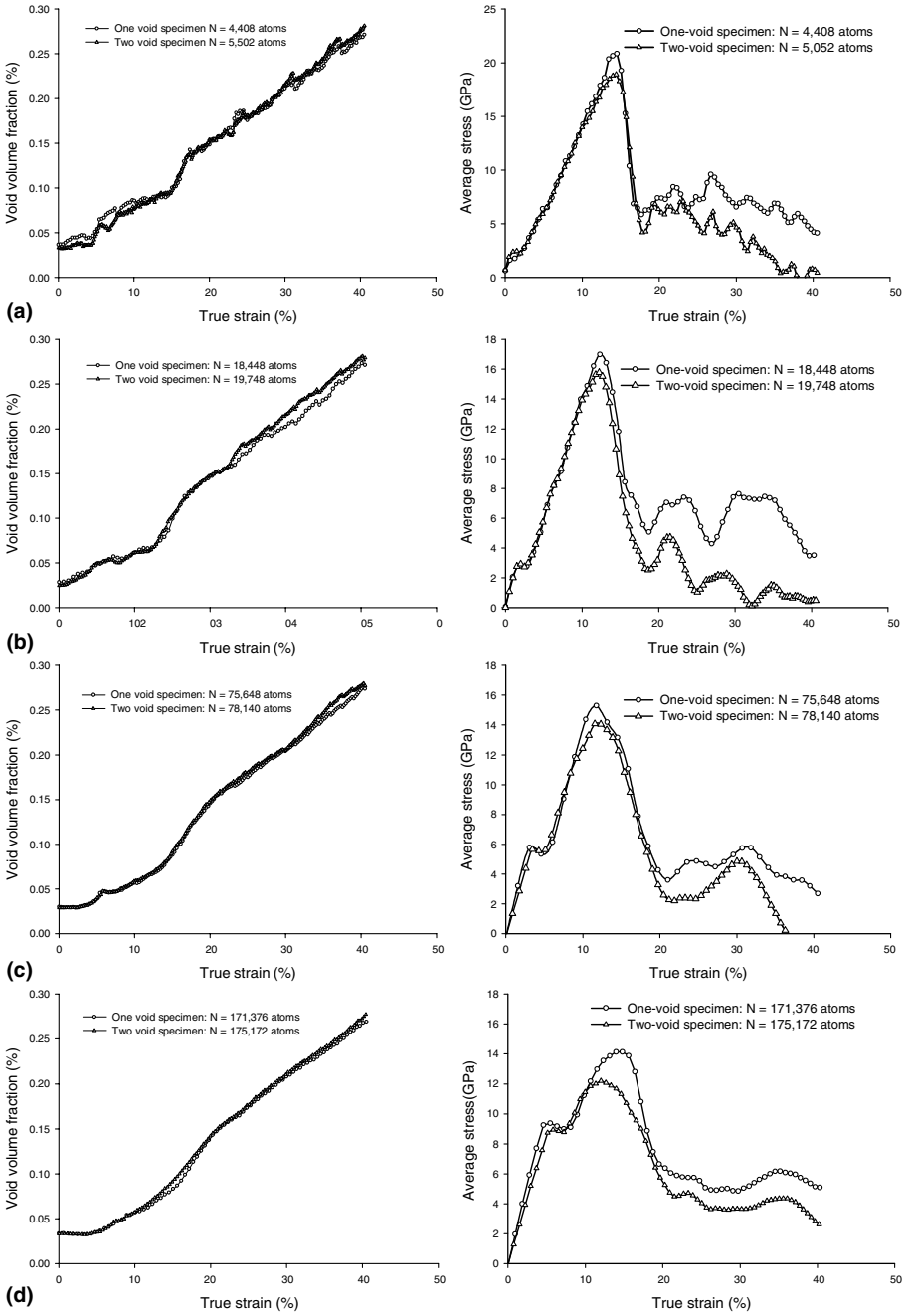

Fig. 9. Comparison between average stress versus true strain responses (10^{10}/s strain rate) due to void growth and void coalescence mechanisms at increasing material length scales: (a) ~5000 atoms; (b) ~19,000 atoms; (c) ~75,000 atoms; (d) ~175,000 atoms.

plastic strains. As the specimens are loaded at large plastic strains, the differences in the void volume evolution for increasing length scales also diminishes, all four increasing length scales showing almost the same void volume fraction variation with the applied uniaxial strain.

4.4. Uniaxial stress–strain responses

The simulations indicate that for the one-void and two-void specimens, material length scale significantly influences the uniaxial stress–strain response. A comparison of the different specimen size stress–strain responses for the one-void and two-void specimens are shown in Fig. 8(a) and (b). Fig. 8(a) shows that for the one-void specimens, as the specimen size increases from 4408 to 171,376 atoms the initial yield decreases monotonically from 20.5 to 14.5 GPa. After the initial yielding of the specimen, the stress–strain response exhibited a sharp stress drop-off. After the initial yielding, the smallest specimen size exhibited in general a higher stress–strain curve. Fig. 8(b) indicates that for the two-void case the initial yield strength decreases monotonically from 18.92 to 12.2 GPa, as the specimen size increases from 5052 to 175,172 atoms.

An important aspect of these results is that the differences observed in the stress–strain curves at increasing specimen size are due to differences in the dislocation nucleation process, since the simulations for the one-void and two-void simulations indicate that the void volume fraction evolution during void growth and void coalescence are practically insensitive to a change in length scale.

In Fig. 9(a)–(d), a comparison between the one-void specimens and two-void specimens at each specimen size is plotted. The plots on the left indicate the evolution of void volume fraction for the two types of specimens, while the plots on the right show the stress–strain response. From Fig. 9(a)–(d), one can observe that the initial yield strength for the two-void specimens is consistently lower than the initial yield strength for the one-void specimens. Also, after the initial yielding, the stress–strain curve is consistently lower for the two-void specimens than for

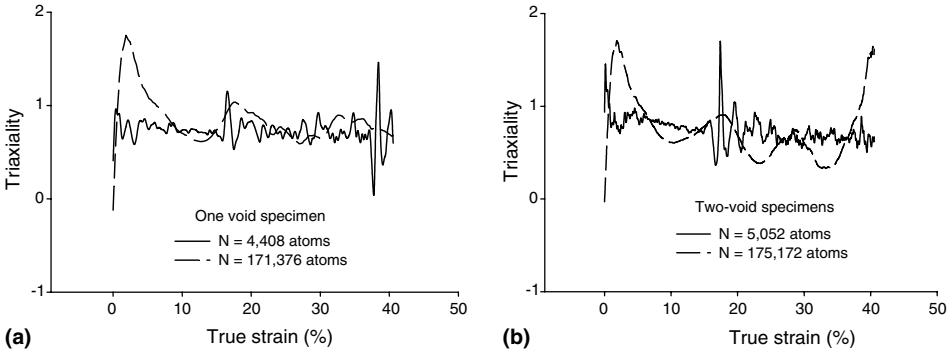

Fig. 10. Triaxiality variation during uniaxial straining at 10^{10}/s strain rate for: (a) one-void specimens; (b) two-void specimens.

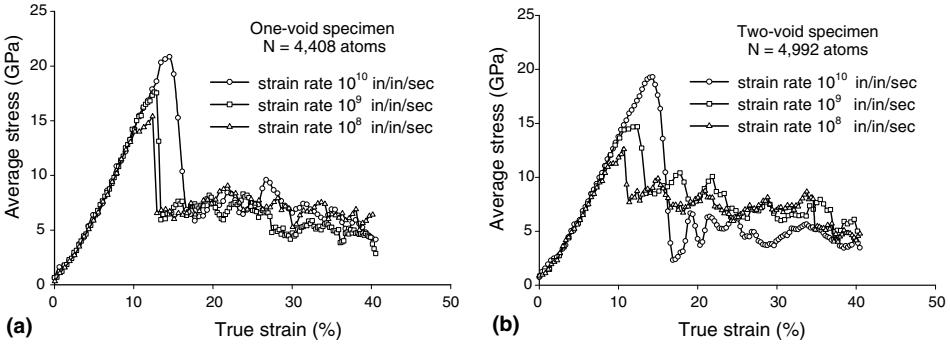

Fig. 11. Influence of strain rate on the average stress versus true strain response for: (a) one-void specimen ($N = 4880$ atoms); (b) two-void specimen ($N = 5052$ atoms).

the one-void specimens. The void volume fraction for the two-void specimens rises more rapidly than that for the one-void specimens toward the end of the loading process.

4.5. Stress triaxiality

The triaxiality (χ), defined as the ratio of the hydrostatic stress to the von Mises stress, has been calculated by averaging the stresses from all the active atoms in the model.

Triaxiality variations with the uniaxial applied strain, at the smallest and the largest specimen sizes are presented in Fig. 10(a) and (b) for the one-void and two-void specimens, respectively. For both cases, the triaxiality values fluctuate around 0.8. The smallest specimen size exhibits a higher frequency oscillatory triaxiality curve than the larger specimen arising from the thermal vibrations having more influence on the stress state in smaller size specimens. Initially, the triaxiality increases significantly in the elastic portion of the loading increasing to values of $\chi = 1.6$–1.8 for an applied strain less than 5%. Afterwards, the triaxiality decreases and saturates at $\chi = 0.7$. The fluctuation of the values for the triaxiality with increasing applied strain is due to the continuous process of dislocation nucleation in the near-void region and increasing necking at the outer edges of the tensile specimen.

4.6. Strain rate effects

Stress–strain responses were obtained for the one-void and two-void specimens at three strain rates levels: 10^8, 10^9 and 10^{10}/s. Due to the intensive computational load and solution times, the smallest specimens were analyzed for the rate sensitivity study. For the one-void specimens, Fig. 11(a) shows that, as the strain rate increased two orders of magnitude, the yield stress increased from 15 to 20.5 GPa. Correspondingly, the elastic strain at which first yielding of the specimen occurred, increased with increasing strain rate. After the initial yielding, the stress–strain

response decreased significantly. Toward final fracture, the lowest stress–strain resistance is exhibited by the specimen that was subjected to the lowest strain rate.

The same qualitative conclusions apply to the analysis of the stress–strain responses for the two-void specimens at the smallest specimen size ($N = 5052$ atoms). The initial yield stress and the elastic strain vary inversely with the rate of deformation.

4.7. Relation to continuum theory

In Horstemeyer et al. (2000b), a macroscopic continuum formulation that delineates void nucleation, void growth, and void coalescence is described by

$$\phi = \eta v c, \tag{6}$$

where ϕ is the total void volume fraction, η is the void nucleation term, v is the void growth term, and c is the void coalescence term. The continuum coalescence function, c, is given by

$$c = 1 + f(\eta, v), \tag{7}$$

which essentially enhances the void growth. This functional form was based on micromechanical finite element simulations (Horstemeyer et al., 2000a), which were performed at low strain rates.

One aspect of this paper is to evaluate if nanomechanical results give similar results as the micromechanical simulations for uniaxial tension. If so, then the continuum theory can be applied down to the nanoscale. If not, then we need to determine the scale dependent features. Because minor differences were observed between one-void and two-void total void volume fractions, as shown in Fig. 9, the coalescence equation shown in Eq. (7) needs to incorporate at least strain rate effects and maybe size scale effects in a direct manner, if the continuum theory is to be applied to nanoscale damage progression.

5. Conclusions

Molecular dynamics simulations showing damage evolution at four increasing specimen sizes were performed to study the evolution of void growth and coalescence under very high strain rates. One-void specimens and two-void specimens were increased in size to represent an increasing length scale. Given that only uniaxial tension of one crystalline orientation free of initial defects was used, the main conclusions are the following:

1. Not much nanoscale coalescence was observed, due probably to the high strain rate effects. Void growth was much more dominant than void coalescence.
2. At the nanoscale, the total void growth is size-scale dependent in the elastic regime but size-independent in the plastic regime.

3. The averaged axial stress–strain response clearly indicated a length scale effect regardless of the number of voids from 0% to 20% strain. The smallest specimen size (length scale) exhibited the largest yield stress.
4. At the nanoscale, the decrease in the stress–strain curve is due mainly to the dislocation nucleation, but no major differences are noticed in the void volume fraction evolution.
5. Even though the initial void volume fraction was the same for all specimens, the differences in plastic slip nucleation pattern indicated a varying void shape evolution as the material length scale was increased. For the one-void specimens, the study revealed that the void embedded in a single crystal grew due to the crystallographic plastic slip that initiated at the hole as a consequence of the stress concentration and propagated toward the outer edges of the specimen. The nucleation and evolution pattern of the plastic slip is highly dependent on the specimen size and hence length scale of (volume per surface area, cf. Horstemeyer, 2001a) the specimen. For the two-void specimens, the study revealed that the configuration of plastic slip also influenced the void coalescence patterns but not the total void volume fractions, depending on the specimen size (length scale).

Acknowledgments

The authors are grateful to the Center for Advanced Vehicular Systems at Mississippi State University for supporting this study. The work of G.J. Wagner and P.M. Gullett is supported by U.S. DOE Contract AC04-94AL85000.

References

Bandstra, J.P., Goto, D.M., Koss, D.A., 1998. Ductile failure as a result of a void sheet instability: Experiment and computational modeling. Mater. Sci. Eng. A, Struct. Mater. Prop. Micro. Proc. 249 (1), 46.

Baskes, M.I., Johnson, R.A., 1994. Modified embedded atom potentials for HCP metals. Modell. Simul. Mater. Sci. Eng. 2, 147–163.

Baskes, M.I., 1994. The modified embedded atom method. Comput. Mater. Model. AD-Vol. 42/PVP-Vol. 294, 23–35.

Baskes, M.I., 1997. Determination of modified embedded atom method parameters for nickel. Mater. Chem. Phys. 50, 152–158.

Benson, D.J., 1993. An analysis of void distribution effects on the dynamic growth and coalescence of voids in ductile metals. J. Mech. Phys. Solids 41 (8), 1285.

Benson, D.J., 1995. The effects of void cluster size on ductile fracture. Int. J. Plast. 11 (5), 571–582.

Bonfoh, N., Lipinski, P., Carmasol, A., Tiem, S., 2004. Micromechanical modeling of ductile damage of polycrystalline materials with heterogeneous particles. Int. J. Plast. 20 (1), 85–106.

Budianski, B.J., Hutchinson, J.W., Slutsky, S., 1982. Void growth and collapse in viscous solids. In: Hopking, H.G., Sewell, M.J. (Eds.), Mechanics of Solids: The Rodney Hill 60th Anniversary Volume. Pergamon Press, Oxford, pp. 13–45.

Chien, W.Y., Pan, J., Tang, S.C., 2004. A combined necking and shear localization analysis for aluminum sheets under biaxial stretching conditions. Int. J. Plast. 20 (11), 1953–1981.

Cocks, A.C.F., Ashby, M.F., 1980. Intergranular fracture during power law creep under multiaxial stresses. J. Metal. Sci. 14 (8), 395–402.

Cocks, A.C.F., Ashby, M.F., 1982. On creep fracture by void growth. Prog. Mater. Sci. 27, 189–244.

Cottrell, A.H., 1959. In: Averbach, B.L., Felbeck, D.R., Hahn, G.T., Thomas, D.A. (Eds.), Fracture. Technology Press of MIT and John Wiley, New York.

Cuitino, A.M., Ortiz, M., 1996. Ductile fracture by vacancy condensation in FCC single crystals. Acta Mater. 44 (2), 427–436.

Daw, M.S., Baskes, M.I., 1984. Embedded-atom method: Derivation and application to impurities, surfaces, and other defects in metals. Phys. Rev. B 29, 6443.

Faleskog, J., Shih, C.F., 1997. Micromechanics of coalescence-I. Synergistic effects of elasticity, plastic yielding, and multi-size scale voids. J. Mech. Phys. Solids 45 (1), 21.

Farrissey, L., Ludwig, M., McHugh, P.E., Schmauder, S., 2000. An atomistic study of void growth in single crystalline copper. Comput. Mater. Sci. 18, 102–117.

Gall, K., Horstemeyer, M.F., Van Schilfgaarde, M., Baskes, M.I., 2000. Atomistic simulations on the tensile debonding of an aluminum–silicon interface. J. Mech. Phys. Solids 48, 2183–2212.

Geltmacher, A., Koss, D.A., Matic, P., Stout, M.G., 1996. A modeling study of the effect of stress state on void linking during ductile fracture. Acta Mater. 44 (6), 2201.

Geltmacher, A., Koss, D.A., Matic, P., Stout, M.G., 1998. Flow localization in sheet specimens with pairs of holes. Met. Trans. A Phys. Metall. Mater. Sci. 29 (3), 775.

Horstemeyer, M.F., 2001. From atoms to autos. A new design paradigm using microstructure-property modeling. Part 1: Monotonic loading. Sandia National Laboratories, SAND2000-8662.

Horstemeyer, M.F., Baskes, M.I., 1999. Atomistic finite deformation simulations: A discussion on length scale effects in relation to mechanical stresses. J. Eng. Mater. Technol. 121, 114–119.

Horstemeyer, M.F., Matalanis, M.M., Sieber, A.M., Botos, M.L., 2000a. Micromechanical finite element calculations of temperature and void configuration effects on void growth and coalescence. Int. J. Plast. 16, 979–1015.

Horstemeyer, M.F., Lathrop, J., Gokhale, A.M., Dighe, M., 2000b. Modeling stress state dependent damage evolution in a cast Al–Si–Mg aluminum alloy. Theor. Appl. Fract. Mech. 33, 49–98.

Horstemeyer, M.F., Baskes, M.I., Plimpton, S.J., 2001a. Length scale and time scale effects on the plastic flow of FCC metals. Acta Mater. 49, 4363–4374.

Horstemeyer, M.F., Baskes, M.I., Plimpton, S.J., 2001b. Computational nanoscale plasticity simulations using embedded atom potentials. Theor. Appl. Fract. Mech. 37, 49–98.

Horstemeyer, M.F., Baskes, M.I., Godfrey, A., Hughes, D.A., 2002. A large deformation atomistic study examining crystal orientation effects on the stress–strain relationship. Int. J. Plast. 18, 203–229.

Horstemeyer, M.F., Baskes, M.I., Prantil, V.C., Philliber, J., Vonderheide, S., 2003. A multiscale analysis of fixed-end simple shear using molecular dynamics, crystal plasticity, and a macroscopic internal state variable theory. Modell. Simul. Mater. Sci. Eng. 11, 265–286.

Kachanov, M.L., 1958. Time of the fractured process under creep conditions. Izv. Akad. Nauk. SSSR OTN Tekh. Nauk. 8, 26.

Kelchner, C.L., Plimpton, S.J., Hamilton, J.C., 1998. Dislocation nucleation and defect structure during surface indentation. Phys. Rev. B 58 (17), 11085–11088.

Lemaitre, J., 1992. A Course on Damage Mechanics. Springer-Verlag, Berlin.

Lu, W.Y., Horstemeyer, M.F., Korellis, J.S., Grishibar, R.B., Mosher, D., 1998. High temperature sensitivity of notched AISI 304L stainless steel tests. Theor. Appl. Fract. Mech. 30, 139.

Makino, M., Tsuji, T., Noda, N., 2000. MD simulation of atom-order void formation in Ni FCC metal. Comput. Mech. 26 (3), 281–287.

McClintock, F.A., 1968. A criterion for ductile fracture by the growth of holes. ASME J. Appl. Mech. 35, 363.

Moran, B., Ortiz, M., Shih, C.F., 1990. Formulation of implicit finite element methods for multiplicative finite deformation plasticity. Int. J. Numer. Meth. Eng. 29, 483.

Nagaki, S., Goya, M., Soweeby, R., 1993. The influence of void distribution on the yielding of an elastic–plastic porous solid. Int. J. Plast. 9, 199–211.

Pardoen, T., Doghri, I., Delannay, F., 1998. Experimental and numerical comparison of void growth models and void coalescence criteria for the prediction of ductile fracture in copper bars. Acta Mater. 46 (2), 541.

Rabotnov, Y.N., 1969. Creep Problems in Structural Members. North-Holland, Amsterdam.

Ramaswamy, S., Aravas, N., 1998. Finite element implementation of gradient plasticity models – Part 1: Gradient dependent evolution equations. Comp. Meth. Appl. Mech. Eng. 163 (1), 33.

Rice, J.R., Tracey, D.M., 1969. On the ductile enlargement of voids in triaxial stress fields. J. Mech. Phys. Solids 17, 201.

Shu, J.Y., 1998. Scale-dependent deformation of porous single crystals. Int. J. Plast. 14 (10-11), 1085–1107.

Tonks, D.L., Thissell, W.R., Zurek, A.K., Hixson, R., 1997. Quantitative Analysis of Damage Clustering in Void Linking for Spallation Modeling in Tantalum. J. de Physique IV France 7 (C3), 841.

Tvergaard, V., 1990. Material failure by void growth to coalescence. Adv. Appl. Mech. 27, 83–151.

Tvergaard, V., Needleman, A., 1995. Effects of Nonlocal Damage in Porous Plastic Solids. Int. J. Solids and Structures 32 (8–9), 1063.

Tvergaard, V., Needleman, A., 1997. Nonlocal Effects on Localization in a Void Sheet. Int. J. Solids and Structures 34 (18), 2221.

Tvergaard, V., Niordson, C., 2004. Nonlocal plasticity effects on the interaction of different size voids. Int. J. Plast. 20 (1), 107–120.

Wen, J., Huang, Y., Hwang, K.C., Liu, C., Li, M., 2005. The modified Gurson model accounting for the void size effect. Int. J. Plast. 21 (2), 381–395.

Worswick, M.J., Pick, R.J., 1995. Void Growth and Coalescence During High Velocity Impact. Mech. of Matls. 19 (4), 239.

Zurek, A.K., Thissell, W.R., Tonks, D.L., Hixson, R., Addesio, F., 1997. Quantification of Damage Evolution for a Micromechanical Model of Ductile Fracture in Spallation of Tantalum. J. de Physique IV France 7 (C3), 903.